OXFORD

Cerebral Cortex, 2023, 1–15
https://doi.org/10.1093/cercor/bhad297
Original Article

Increased noise relates to abnormal excitation-inhibition balance in schizophrenia: a combined empirical and computational study

Samira Abbasi[1,2,*], Annemarie Wolff[1], Yasir Çatal[1], Georg Northoff[1]

[1]University of Ottawa, Institute of Mental Health Research, Ottawa ON K1Z 7K4, Canada,
[2]Department of Biomedical Engineering, Hamedan University of Technology, Hamedan 65169-13733, Iran

*Corresponding author: Royal Ottawa Mental Health Centre, 1145 Carling Avenue, Rm. 6435, Ottawa, ON K1Z 7K4, Canada. E-mail: samira.abbasi@gmail.com

Electroencephalography studies link sensory processing issues in schizophrenia to increased noise level—noise here is background spontaneous activity—as measured by the signal-to-noise ratio. The mechanism, however, of such increased noise is unknown. We investigate if this relates to changes in cortical excitation-inhibition balance, which has been observed to be atypical in schizophrenia, by combining electroencephalography and computational modeling. Our electroencephalography task results, for which the local field potentials can be used as a proxy, show lower signal-to-noise ratio due to higher noise in schizophrenia. Both electroencephalography rest and task states exhibit higher levels of excitation in the functional excitation-inhibition (as a proxy of excitation-inhibition balance). This suggests a relationship between increased noise and atypical excitation in schizophrenia, which was addressed by using computational modeling. A Leaky Integrate-and-Fire model was used to simulate the effects of varying degrees of noise on excitation-inhibition balance, local field potential, NMDA current, and . Results show a noise-related increase in the local field potential, excitation in excitation-inhibition balance, pyramidal NMDA current, and spike rate. Mutual information and mediation analysis were used to explore a cross-level relationship, showing that the cortical local field potential plays a key role in transferring the effect of noise to the cellular population level of NMDA.

Key words: schizophrenia; EEG; noise; local field potential; NMDA current.

Introduction

Imagine yourself having a conversation at a party. Standing among the other guests, you strain to hear what your friend is saying. The background chatter drowns them out; they ask you questions, but you can't always hear them clearly, so you don't always respond. This example of important stimuli in your environment being drowned out by irrelevant background activity illustrates what subjects with schizophrenia (SCZ) may experience more intensely than healthy individuals. Though many studies have shown impaired sensory processing in SCZ (Javitt 2009; Lakatos et al. 2009, 2013; Palaniyappan et al. 2013; Javitt and Freedman 2015; Martínez et al. 2015; Thoenes and Oberfeld 2017), the underlying mechanism of this impairment is still unknown.

A few electroencephalography (EEG) studies (Winterer et al. 1999; Winterer et al. 2000; Wolff et al. 2022) have provided evidence that the source of this impairment is an increase of the ongoing spontaneous neural activity. This spontaneous neural activity—here termed task-irrelevant neuronal "noise" (David et al. 2006) (as distinct from artifact noise (Faisal et al. 2008))—co-occurs with activity evoked by a stimulus, here termed "signal." A lower ratio of these two components (as measured by the signal-to-noise ratio or SNR) has been seen in participants with SCZ in multiple tasks, sensory modalities, and datasets, along with higher noise (Winterer et al. 2000; Winterer and Weinberger 2004; Molina et al. 2016; Wolff et al. 2022). What, though, are the neuronal and computational mechanisms of such altered SNR with increased noise in SCZ? Addressing this open question is the goal of our study.

One key feature in mediating changes from the cellular level to the more systemic level is the excitation-inhibition balance (EIB; Anticevic et al. 2015; Sohal and Rubenstein 2019; Adams et al. 2022; Friston 2022). Various studies using computational modeling (Rolls et al. 2008; Qian et al. 2020), molecular investigations (NMDA, GABA) in animal models (Kehrer et al. 2008; Davenport et al. 2019), and human PET (Narendran et al. 2020) studies suggest an atypical EIB with abnormally increased excitation in SCZ. Despite this work, it is unknown whether EIB abnormalities in SCZ can be measured directly, such as at the systemic level of EEG. Moreover, given that noise can be observed in EEG (Winterer et al. 1999; Winterer et al. 2000; Winterer et al. 2004; Wolff et al. 2022), a close relationship between abnormal EIB and increased noise in SCZ can be hypothesized.

To investigate the relationship of noise and EIB in SCZ, we here uniquely combine empirical EEG data at the systemic level with computational modeling at the neural population level. For the first time, we measure both SNR/noise and EIB in EEG recordings of SCZ participants. This is complemented by computational modeling which, using a neural population network (based on the Leaky Integrate-and-Fire (LIF) model (Gerstner and Kistler 2002)), demonstrates causal relationship of increased noise with abnormally high excitation in the EIB. The link of systemic EEG and the cellular-population model was established by local field potentials (LFPs), which provide the physiological basis of the EEG

Received: May 29, 2023. **Revised:** July 25, 2023. **Accepted:** July 26, 2023

signal (Friston et al. 2015). The LFP reflects the summation of the extracellular electrical field of many neurons (Nunez and Srinivasan 2006; Buzsáki et al. 2012). In a population of cortical pyramidal neurons, this can be modeled as the sum of the absolute values of inhibitory and excitatory currents (Mazzoni et al. 2008, 2010, 2011). The LFP can thus be measured at the level of a population of pyramidal neurons, and so can serve as proxy for the EEG recording in a computational model (Glomb et al. 2022).

The goal of our study is to investigate the changes in SNR and EIB, including their relationship in SCZ. For that, we combine empirical EEG measures (SNR, functional excitation-inhibition ratio or fE/I) and analogous measures (SNR, EIB) (and other more cellular; NMDA current, spike rate or SR) in the population-based computational model. Our first specific aim was to investigate amplitude in event-related potentials (ERPs), SNR, and EIB on the more systemic level of EEG resting state and two different tasks, including an auditory oddball task. We had two hypotheses: (i) SCZ participants would have lower peak amplitude in the task-relevant stimulus (deviant) compared with healthy controls; and (ii) the SNR in SCZ participants would be lower than healthy controls due to higher noise rather than reduced signal. Furthermore, for the first time, we measured the fE/I (Bruining et al. 2020) in human EEG data of SCZ participants. We hypothesized that participants with SCZ would have a higher fE/I with higher levels of excitation than healthy controls; according to the NMDA hypothesis, greater NMDA receptor hypofunction would lead to greater excitation (Jami et al. 2021) and, as per our hypothesis, increased noise.

To examine and quantify the relationship of noise and EIB, we simulated a neural population network comprised of pyramidal cells and interneurons. Such networks have been extremely popular as simplified models of local networks in the neocortex (Ledoux and Brunel 2011). The network was simulated based on the LIF model; it is usually used in simulation studies (Brunel 2000; Gerstner and Kistler 2002). In this network, noise refers to the background spontaneous activity in the cortex (Chance et al. 2002; Calvin and Redish 2021) arising from randomly-timed excitatory inputs to pyramidal and interneuron populations, thus affecting the activity of these populations (Calvin and Redish 2021). There is agreement that this background activity is mediated through AMPA receptors (Wang 1999; Compte et al. 2000; Vierling-Claassen et al. 2008; Deco et al. 2014; Calvin and Redish 2021). This AMPA receptor mediation is modeled as an uncorrelated Poisson process (Wang 1999; Brunel 2000; Compte et al. 2000; White et al. 2000; Vierling-Claassen et al. 2008; Ledoux and Brunel 2011; Deco et al. 2014; Murray et al. 2014; Zou and Wang 2016; Calvin and Redish 2021).

This neural network simulation was done to probe the effect of varying strengths of input current (serving as a proxy for noise) to pyramidal and interneuron neural populations. From the resulting activity of the neural population network, we measured the (i) excitation-inhibition ratio (EI ratio), (ii) LFP, (iii) NMDA current, and (iv) SR of the pyramidal population. Given that the LFP (as the bridge to EEG) are mainly mediated by pyramidal cells rather than interneurons (Martínez-Cañada et al. 2021), we focused our measurements on pyramidal cells.

We hypothesized that increasing degrees of noise applied to pyramidal population would lead to (i) higher levels of excitation in EIB, (ii) stronger LFP, (iii) greater NMDA current, and (iv) increased SR thus entailing a causal relationship between noise and EIB/LFP.

Cross-level relationships of the cellular population level of NMDA with the cortical level of EIB and LFP were substantiated by mediation analysis and further by calculating mutual information (MI) and dynamic time warping (DTW) during varying degrees of noise. This was driven by our hypothesis that increasing degrees of noise lead to changes in the EIB and especially its excitatory component (Anticevic et al. 2015), which, in turn, relates to both the cellular population level of NMDA currents and the cortical level of the LFP. This bidirectional approach—from the systemic level of EEG recordings to the cortical level of the LFP (bottom-up; Dalal and Haddad 2022), and from the cellular population level of the neural network activity to the cortical level of the LFP (top-down; Dalal and Haddad 2022)—allows us to connect these two methodologies through the LFP.

A general schematic diagram of this study is shown in Fig. 1.

Materials and methods

EEG analysis

EEG datasets

Each participant in the EEG datasets provided written informed consent prior to the acquisition of data. In addition, the use of the included datasets and analyses in this study were approved by the Research Ethics Board of the Institute of Mental Health Research at the University of Ottawa (REB # 2021002). All EEG data were recorded using a Brain Vision EasyCap with 32 Ag/AgCl electrodes at a sampling rate of 500 Hz. Electrode AFz served as the ground and an additional nose electrode served as the reference during recording. Additional channels were added to increase the accuracy of the independent component analysis (ICA) decomposition: vertical ocular (above and below the left eye), and horizontal ocular (the outer canthi of the right and left eyes). The impedance of all channels was maintained at less than 5kΩ during recording.

For the functional excitation-inhibition balance (fE/Ib) analyses, three types of continuous EEG data were used. Resting-state data were first. Prior to beginning the tasks, participants completed 3-min resting-state EEG recordings with their eyes closed (Jaworska et al. 2018). These three continuous minutes of eyes closed resting state data was used for the fE/Ib analysis.

Next, the EEG activity from an auditory oddball task (Jaworska et al. 2013) was isolated. The task was presented to participants using Presentation software (Neurobehavioral Systems, Albany, CA, USA). Participants were presented with 800 tones. Eighty percent of the tones—standards—were 1,000 Hz and 70 -B pure tones 336 ms in length. Ten percent (80) were deviant tones at 700 Hz (70-dB pure tones lasting for 336 ms, identical to standards). Participants were instructed to respond to the deviant tones by a button press. The remaining 10% (80) were novel non-target—participants did not respond by a button press—environmental sounds (i.e. dog bark, horn, etc.) at 65–75 dB for 169–399 ms. The intertrial interval between stimuli was 1 s. To match the 3 min of resting state, 3 min of continuous activity from the middle of the task was isolated and used for fE/Ib analysis.

Finally, the third type of data used in the fE/Ib computation was an auditory gating task (Choueiry et al. 2019). Only data from the first placebo session were used; therefore, there was no effect of medication in this data. One hundred and twenty *a*-*a* vowel pairs (/a/; $F = 140$ Hz; 170-ms duration) were administered binaurally through headphones at 80 dB (SPL). Vowel pairs (*a*-*a*; S1–S2) were presented at intra-pair intervals of 0.5 s and inter-pair intervals of 10 s. During the paradigm presentation, patients were instructed to ignore the sounds and to visually fixate on the center of a black computer screen while remaining seated and relaxed. As was done in the auditory oddball data, 3 min of continuous

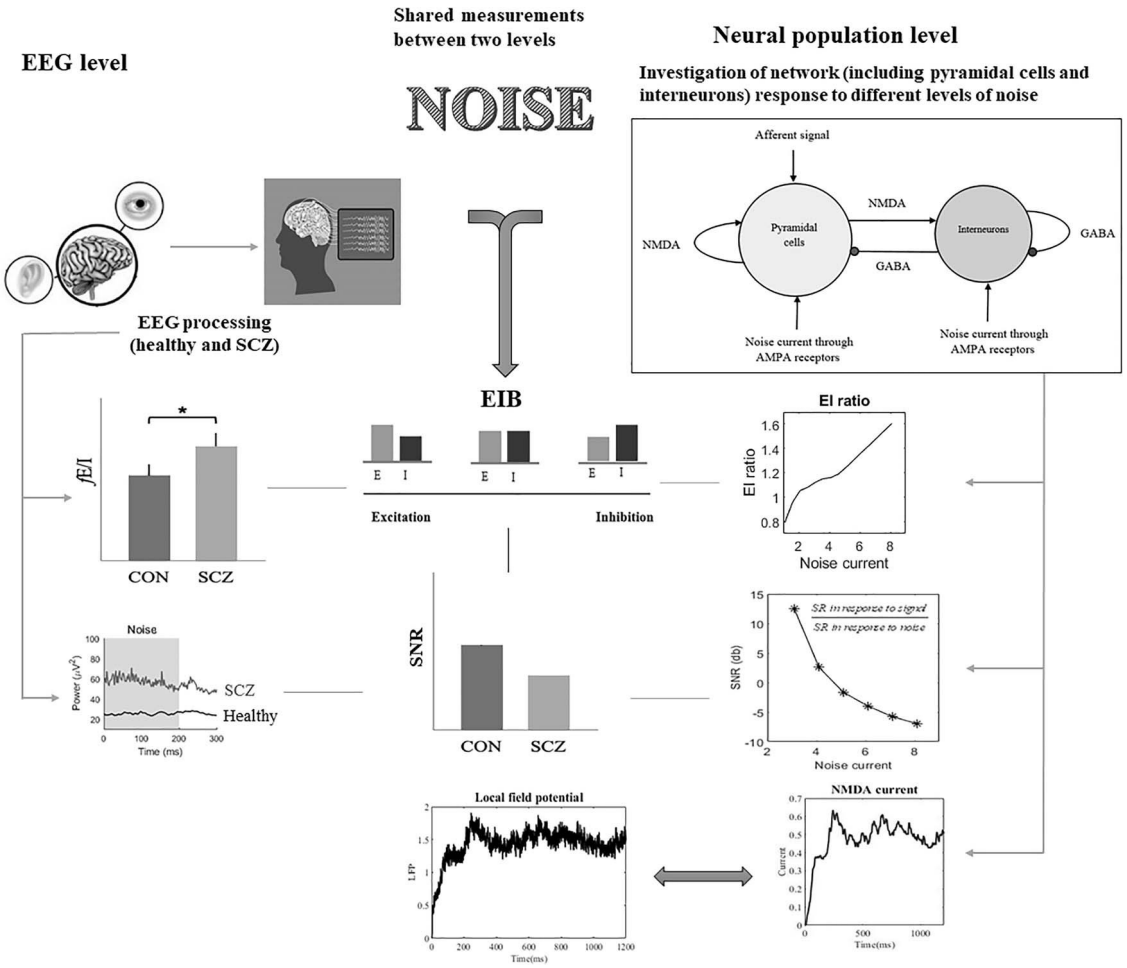

Figure 1. General diagram showing different levels of analyses. The left side represents the macroscale level or EEG level with actual data from human participants; the right part represents the microscale level of our neural population with simulated data, and the center shows common measurements between the two levels. Left part: EEG recording of healthy control and SCZ subjects. EEG data revealed decreased SNR in SCZ compared with healthy subjects. A significantly lower SNR has been found in SCZ participants compared with healthy controls in several publications (Winterer et al. 1999, 2000; Winterer and Weinberger 2004; Wolff et al. 2022), and here we replicated those results. Also, *f*E/I was measured, and results showed enhanced *f*E/I in SCZ compared with the healthy (control) group. Right side: neural population level simulation data. The box (top) represents a schematic of the network architecture. Arrows and filled circles in this network indicate excitatory and inhibitory connections, respectively. Neurons receive the noise current through AMPA receptors, and each neuron receives its own noise realization, independent of that received from others. Afferent current for interneurons is zero and it is applied only to pyramidal cells. Different strengths of noise were applied to the populations and NMDA current, SR, EI ratio, LFP, and SNR were measured. Middle part: shared measurements between neural population network and EEG levels. LFP (bottom), EI ratio, and SNR were measured in both levels.

activity from the middle of the task was isolated and used for *f*E/Ib analysis.

EEG preprocessing

All EEG data preprocessing was completed using EEGLAB (v2019) (Delorme and Makeig 2004). This required MATLAB (The MathWorks) v2018a, including the use of the Optimization, Statistics, and Signal Processing Toolboxes. To ensure that our findings were not due to any artifacts from the hardware or recording of the EEG data, we employed a rigorous preprocessing regime to remove as many artifacts from the EEG data as possible prior to beginning analysis.

Raw EEG data were imported to EEGLAB. The continuous data were then low- and high-pass Hamming windowed sinc Finite Impulse Response (FIR) filtered from 0.1 to 80 Hz. Flat and noisy electrode channels were then removed. Flat electrode channels were removed if they were flat longer than 5 s. Noisy channels were removed if they had the following properties: correlation of mean over 5 s of less than 0.85 with other channels (Bigdely-Shamlo et al. 2015); mean value over 5 s greater than 4 standard deviations (SD) from the mean of all channels. The removed channels were then spherically interpolated.

Cleanline (Mullen 2012) at 60 Hz was then used to remove electrical line noise. The parameters were sliding window length and step of 4 s (no overlap), default smoothing factor of 100, default *P*-value of 0.01 for detecting significant sinusoid, and an FFT default padding factor of 2. After cleanline was used, the EEG data were re-referenced to the average activity of all channels.

Finally, all stationary artifacts, specifically eye movements (blinks and saccades), were reduced using ICA and the Multiple Artifact Rejection Algorithm (MARA; Winkler et al. 2011; Winkler et al. 2014). MARA is a plug-in associated with EEGLAB that uses a supervised machine learning algorithm—the model was trained on expert ratings of 1,290 components—to label ICA components with a probability of being an artifact. If the probability is greater than 50%, the artifact is automatically rejected.

ERPs, SNR, signal, and noise

For the ERP and SNR analyses, the data from the auditory oddball task (as described above) was used. Only the standard and deviant stimuli were used, with a baseline of −400 ms before stimulus onset to stimulus onset. Sixty randomly selected trials for both stimuli were used for each participant. Both the ERP, the SNR, and the signal and noise were computed at one electrode according to methods (Wolff et al. 2022) studies: Pz for the ERP (Jaworska et al. 2013) and Fp1 for the SNR, signal, and noise (Wolff et al. 2022). For the ERP, the maximum amplitude between 300 and 600 ms was measured. For the SNR, signal and noise, the area-under-the-curve (AUC) between 0 and 200 ms was calculated.

Functional excitation-inhibition balance computation

After preprocessing the resting state, and the auditory oddball and gating task data, 3 min of continuous data were isolated from each file for the *f*E/Ib computation. This was done as the resting state data was 3 min long; therefore, the two task blocks were cut to have the same length, with the 3 min isolated from the middle of the blocks.

The *f*E/Ib was computed according to the methods of Bruining et al. (Bruining et al. 2020) and using their MATLAB function, which is located at https://github.com/rhardstone/fEI. In their recent paper (Bruining et al. 2020), a method to quantify an *f*E/Ib in human EEG data was shown. This computation of *f*E/Ib is done from neuronal oscillations, specifically in the alpha frequency band (8–13 Hz). Briefly, the alpha band filtered amplitude envelope of continuous activity is first demeaned. The continuous activity is then split into windows of 5 s and 80% overlap, with each window being normalized by its mean. Each window is then detrended, and the SD of each window is calculated. This is then known as the normalized fluctuation function (nF(*f*)) and serves as a proxy for long-range temporal correlations on short timescales and amplitude. The *f*E/Ib is the calculated as one minus the Pearson correlation coefficient between all nF(*f*)s and all windowed amplitude values.

To remain consistent with the methods of the above paper, the data were first re-referenced to Cz. Next, the continuous data were filtered in the alpha range (8–13 Hz) using MATLAB function *bandpass*. The reason we first filtered the data in the alpha range of 8-13 Hz was to follow the methods of Bruining et al (Bruining et al. 2020) exactly. In their methods section (preprocessing and analysis of EEG data, page 12), Bruining et al state that they extracted the alpha band amplitude envelope between 8 and 13 Hz for all subsequent analyses, so we did the same to maintain consistency with their method.

The absolute value of the Hilbert transform was then extracted and served as input to the *f*E/I function. The window length of the sliding window was 5 s, with an overlap of 0.8, which are the same parameters used in the original publication for *f*E/I (Bruining et al. 2020). As this was the first known application of the fE/I method to another clinical group (schizophrenia), in order to get the best comparison with their results, we followed their method to the letter.

This calculation was done for all 32 channels.

Neural network population modeling

Network simulation

The computational modeling approach was used to investigate the effect of background noise on the network response. To study the dependence of the network activity in response to different strengths of the noise current, we simulated a neural population network and measured NMDA current, EI ratio, SR, LFP, and SNR. To determine different levels of correlation and relationship, Pearson's correlation and mediation analysis were used. Then, MI was computed to probe if these measurements share information. DTW was used as a confirmation of the MI results.

To check if different factors which leads to increased EI ratio cause similar relationship, more simulations were done in the next step by changing GABA receptor conductance. We expected a reduction in pyramidal GABA conductance increases the EI ratio and changes both LFP and NMDA current. So, we controlled if here LFP and NMDA have similar relationship to previous simulations, and we repeated all analysis for it.

A network model based on previous studies (Wang 1999; Compte et al. 2000; Murray et al. 2014; Calvin and Redish 2021) was implemented, with the network architecture as depicted inside the top right box in Fig. 1. The network consisted of two populations, one of excitatory pyramidal cells and another of inhibitory interneurons. Simulations include 1,024 (N_E) pyramidal cells and 256 (N_I) interneurons, yielding a ratio of $N_E/N_i = 4$.

To simulate network activity, we used LIF model neurons which is a popular model to simulate neural populations (Brunel 2000; Gerstner and Kistler 2002). The transmembrane voltage of each neuron obeys the following current balance equation:

$$C_m \frac{dV_m}{dt} = -I_{Leak} - I_{NMDA} - I_{GABA} - I_{Aff} - I_{Noise} \quad (1)$$

where C_m represents the membrane capacitance, V_m is the membrane voltage, I_{GABA} is the current from GABA receptors, I_{NMDA} represents the current from NMDA receptors, and I_{Leak} is the leaky membrane current. I_{Aff} is the current from afferent neurons, and I_{Noise} is the current caused by noisy cell firings impinging on this neuron, mediated by AMPA receptors. In the present study, the effect of change in I_{Noise} on the network output was investigated.

Neurons receive their recurrent excitatory inputs through AMPA and NMDA receptors and their inhibitory inputs through GABA receptors.

When V_m reaches the threshold voltage V_{th}, the neuron is said to generate an action potential and release neurotransmitters onto other downstream neurons. After generating an action potential, the interneuron or pyramidal cell enters an absolute refractory period (τ_{ref}). When the neuron returns to its resting potential (V_{rest}), the absolute refractory period ends. The neuron specific parameters are given in Table 1. Model parameters are taken from reference (Calvin and Redish 2021).

The voltage-dependent leak current is modeled as

$$I_{Leak} = g_L (V_m - V_L) \quad (2)$$

where V_L is the reversal potential of the leak channels, and g_L is the passive membrane conductance. The leak current parameters are indicated in Table 1.

The current from NMDA receptors was given by

$$I_{NMDA} = \frac{g_{NMDA} s_{NMDA} (V_m - V_E)}{1 + [Mg]\, e^{-0.062 V_m}/3.57} \quad (3)$$

where g_{NMDA} represents the receptor conductance, s_{NMDA} is the gating variable (the fraction of receptors in the open state), V_E is the synaptic reversal potential, and $[Mg]$ is the concentration of Mg^{2+} (magnesium) ions in the extracellular fluid. Channel

Table 1. Different parameters of the model and its receptors.

Model parameter	Value
V_{th} for all neurons	−50 mV
V_{rest} for all neurons	−60 mV
τ_{ref} for all neurons	2 ms
V_I for all neurons	−70 mV
C_m for pyramidal cells	0.5 nF
C_m for interneurons	0.2 nF
V_L for all neurons	−70 mV
g_L for pyramidal cells	25 nS
g_L for interneurons	20 nS
NMDA receptor	
Parameter	**Value**
V_E	0 mV
[*Mg*]	1 mM
α_x	1 ms^{-1}
τ_x	2 ms
α_s	1
τ_s	80 ms
g_{NMDA} for pyramidal cells	370 nS
g_{NMDA} for interneurons	300 nS
GABA receptor	
Parameter	**Value**
V_I for all neurons	−70 mV
τ_I for all neurons	10 ms
g_{GABA} for pyramidal cells	1.25 uS
g_{GABA} for interneurons	1 uS
AMPA receptor	
Parameters	**Value**
V_E	0 mV
τ_{AMPA}	2 ms
Noise firing rate	1.8 kHz

kinetics is modeled by

$$\frac{dx}{dt} = \alpha_x \sum_i \delta\,(t - t_i) - x/\tau_x \tag{4}$$

$$\frac{ds}{dt} = \alpha_s x\,(1 - s) - s/\tau_s \tag{5}$$

where δ shows Dirac delta function; x is an intermediate gating variable, and s is the fraction of open channels. The t_i are the presynaptic spike times indexed by the spike number i. τ_x is the mean lifetime of the receptors changing from the closed-to-open state, and in fact controls the rise time of NMDA receptors channel conductance. τ_s is the mean lifetime of the receptors changing from the open-to-closed states and is the decay time of NMDA currents. α_x is the jump in value of the x kinetic with each received spike, and α_s controls the saturation of the receptor.*NMDA receptor parameters as indicated in Table 1*. The currents from GABA receptors were modeled using first-order kinetics:

$$I_{GABA} = g_{GABA}\, s_{GABA}\ (V_m - V_I) \tag{6}$$

where g_{GABA} is the receptor conductance, s_{GABA} is the synaptic gating variable, and V_I is the synaptic reversal potential. The gating variable s_{GABA} was simulated using first-order kinetics, and increases by the weight of the connection with each presynaptic action potential and exponentially decreases otherwise. It is governed by

$$\frac{ds}{dt} = \alpha_I \sum_j \delta\left(t - t_j^-\right)(1 - s) - s/\tau_I \tag{7}$$

where t_j^- is presynaptic spike time, i.e. the summation is over presynaptic spike times. α_I controls the rate of increase of s at each incoming spike, and is set to 1, whereas τ_I is its average life expectancy. GABA receptor parameters are indicated in Table 1. In this study, the effect of reduction in GABA receptor conductance on each population was examined, as well to see how the network respond to these alterations. For this purpose, the conductance was reduced to zero in steps of 20% of baseline value (1.25 uS for pyramidal cells and 1 uS for interneurons).

I_{aff} is the current from afferent signals, i.e. other neurons in the EI network, and equally affects the entire excitatory population. In simulations, this current was considered steady over time and set to 0.3 nA for pyramidal cells and zero for interneurons (Calvin and Redish 2021).

The background activity or noise current I_{Noise}, usually is modeled as an uncorrelated excitatory Poisson process (Brunel 2000; White et al. 2000; Vierling-Claassen et al. 2008; Ledoux and Brunel 2011; Deco et al. 2014; Zou and Wang 2016; Calvin and Redish 2021), and mediated through AMPA receptors (Wang 1999; Compte et al. 2000; Vierling-Claassen et al. 2008; Deco et al. 2014; Calvin and Redish 2021). This current was given by the equation:

$$I_{Noise} = g_{Noise}\, s_{AMPA}\ (V_m - V_E) \tag{8}$$

where g_{Noise} is the receptor conductance, s_{AMPA} (the fraction of open channels) is the synaptic gating variable, and V_E is the synaptic reversal potential. The kinetic was modeled as a first-order (similar to GABA kinetics) that increased by the weight of the connection from each spiking presynaptic pyramidal cell and exponentially decreased otherwise. It was assumed that excitatory postsynaptic potentials caused by noisy incoming spikes were uncorrelated with each other (Wang 1999; Brunel 2000; Compte et al. 2000; Deco et al. 2014; Murray et al. 2014; Calvin and Redish 2021) and arrived at a mean rate of 1.8 kHz to each neuron (Calvin and Redish 2021).*AMPA receptor parameters are shown in Table 1*. As shown in Equation (8), the amplitude of the current is proportional to the conductance. Interneuron noise conductance is 2.38 nS, and pyramidal noise conductance is 3.1 nS. We consider this condition as a baseline state (default network model). To change the noise current applied to the pyramidal and interneuron populations, their noise conductance is changed in steps of 0.5 nS to obtain values lower and higher than the baseline state, and the output activity is analyzed for each setting. Conductance does not exceed 10 nS (White et al. 2000); therefore, in this study, it was varied between 1.6 and 8.1 nS for pyramidal cells and between 0.38 and 7.38 nS for interneurons. Within this range, where neurons are not silent, they exhibit asynchronous firing patterns (refer to Supplementary Fig. 7).

In the original model (Calvin and Redish 2021) on which our study is based, AMPA receptor conductance from intra-circuit connections were not modeled, as it was found that activity could be maintained without them (Deco et al. 2014). Their inclusion would entail unnecessary complications in the modeling of the excitatory and inhibitory balance (Calvin and Redish 2021). However, the noise current (I_{Noise}) in the model is considered to be mediated by AMPA receptors (Wang 1999; Compte et al. 2000; Vierling-Claassen et al. 2008; Deco et al. 2014; Murray et al. 2014; Calvin and Redish 2021).

Network architecture

The network was simulated with all-to-all connectivity. Connection weights between presynaptic and postsynaptic neurons from

one neural population to itself or another population were normalized such that the sum of connection weights to any given neuron from a population was set to 1 (Calvin and Redish 2021).

Simulations

Changes in membrane voltages and receptor kinetics were integrated using the second-order Runge–Kutta method. The integration time step was set to 0.01 ms. All neural networks were constructed in Python 3. Some of the analyses were done in MATLAB R2018b.

Simulations were run for 1,200 ms, and the first 200 ms was omitted in the analysis to exclude the transient part. Characteristics of the simulated network were assessed in the remaining 1,000-ms interval. However, to assure that the response does not change over longer time scales, some simulations were repeated for 5,000 ms. Simulations were repeated for five runs, i.e. five different realizations of the noise process. The following were extracted from pyramidal population output for each simulation (averaging across five runs): NMDA current, EI ratio, SR, LFP, and SNR.

NMDA current

This current is modeled by equation (3), and the mean across the pyramidal population was measured.

Excitation-inhibition ratio

The excitation inhibition ratio was defined as the mean of excitatory currents on pyramidal cells divided by the mean of inhibitory current on pyramidal cells (Lam et al. 2022) (i.e. summation of the mean values of NMDA and noise currents divided by mean of GABA current).

Spike rate

SR represents the mean number of spikes per second, and quantifies the neuronal activity (Braun et al. 2022).

Local field potential

We employed a conventional approach to compute LFP, which has been widely utilized in prior research studies (Mazzoni et al. 2008, 2010, 2011). The LFP was defined as the sum of absolute values of NMDA and GABA currents on the pyramidal population (Mazzoni et al. 2008, 2010, 2011).

Signal-to-noise ratio

To assess the SNR at the neural population level, we utilized a pulse waveform as our signal. The pulse had a duration of 250 ms and an amplitude of 0.25 nA (Fig. 5A). Following 700 ms of simulations, the pulse was applied to the pyramidal population. We subsequently computed the SNR by comparing the average SR of the pyramidal population in response to the signal with that of the background noise. The calculation of SNR is represented by Equation (9):

$$SNR = 10 \times \log_{10} \frac{mean\ SR\ in\ response\ to\ signal}{mean\ SR\ in\ response\ to\ noise} \tag{9}$$

Mediation analysis

After measuring NMDA, EI ratio, SR, and LFP, we did mediation analysis to investigate their relationships.

Two models of relationship between an independent variable (x) and dependent variable (y) are illustrated in Supplementary Fig. 1. The total effect or simple association between two variables of x and y is shown in Supplementary Fig. 1(A), which indicates the independent variable affects the dependent variable directly. Supplementary Fig. 1(B) depicts mediation model. Mediation models are useful to investigate whether an association between two variables is transmitted via a third variable (mediator) (Shrout and Bolger 2002). In many systems, the relationship between two variables, x and y, may be transferred through a third intervening variable (Supplementary Fig. 1B). This variable is called the mediator (m). In the mediation model, x is called the initial variable, and y is the outcome or dependent variable. A mediation model path diagram, with standard notation for path coefficients (a, b, a^*b, and c'), is shown in supplement Fig. 1. The coefficient of path from x to y without mediator (total effect) is c. The coefficients of paths from x to m, m to y, and the direct path from x to y with controlling for the mediator are presented by a, b, and c', respectively. The coefficient of the indirect path from x to y is a^*b. If the indirect effect is statistically significant, then m is considered a mediator (Lemardelet and Caron 2022). If indirect effect is significant but the direct effect controlling for the mediator is not significant, then full mediation occurs. If both are significant, this suggests partial mediation. Standard errors (SE) are shown in parentheses.

In this paper, the M3 MATLAB toolbox was used to do mediation analysis (Shrout and Bolger 2002; Kenny et al. 2003). We aimed to test how the effect of alterations in EI ratio (as a key parameter for network function; Anticevic et al. 2015) is transferred to either NMDA current or LFP. The significance of mediation results was tested with the bootstrapping method with 10,000 bootstraps as implemented in the aforementioned M3 toolbox.

Before doing mediation analysis, Pearson's correlation between all the variables (NMDA current, EI ratio, SR, and LFP) was calculated and its significance was explored.

Mutual information

Information theory states that if two variables are related and one of them is known, information reduces uncertainty in the other variable. (Timme and Lapish 2018). This reduction in uncertainty is called MI. In other words, MI measures the amount of shared information in two variables. In addition, it can measure nonlinear interactions, so is not restricted to monotonic relationships. This is the advantage of MI in comparison to Pearson's or Spearman's correlations. Pearson's correlation can just measure linear dependence, whereas Spearman's correlation is limited to monotonic non-linear dependences. In contrast, MI measures general dependence, including linear and non-linear dependence (Kraskov et al. 2004; Timme and Lapish 2018).

With an important role in neuroscience, MI can quantify the information in the nervous system (Dimitrov et al. 2011). MI is defined by equation (10):

$$MI(I,J) = \sum_{i \in I} \sum_{j \in J} p(i,j) \log_2 \frac{p(i,j)}{p(i)p(j)} \tag{10}$$

where $MI(I,J)$ represents the MI between two variables i and j; $p(i)$ and $p(j)$ are marginal probabilities, and $p(i,j)$ is the joint probability of the values i and j. The MI is symmetric, i.e. $MI(I,J) = MI(J,I)$, and it is the same as entropy for $I = J$ (Kraskov et al. 2004).

In this study, we use MI to measure the amount of shared information between each key variables in response to different strengths of noise current. The MI was calculated using PyInform library in Python 3.

A shuffling approach was used to determine that the MI results are significant and not random. To shuffle we changed the order for the series that were used in the MI function randomly, and then calculated the MI. We did this for 1,000 times and then got the significant range for these random correspondences. Finally, we checked if the original results differ from the shuffled results significantly.

Dynamic time warping

DTW measures similarity, and it is among the most common measurements of similarity. DTW is a distance-based measurement between two sequences, and it calculates an optimal match between given sequences (Tao et al. 2021).

DTW aligns elements in two sequences and calculates the Euclidean distance between aligned elements. Actually, it finds the best or optimal match between sequences by minimizing a cost. The cost is defined as the sum of the absolute Euclidean distance (Salvador and Chan 2007). The optimal match between two sequences satisfies the various rules and restrictions (Webb and Petitjean 2021) which were met by our data and followed in our analyses.

In this study, we used DTW to confirm MI results. In addition, to avoid the effect of different ranges of variables on DTW, at first, values were normalized by dividing by the maximum in each variable. DTW was then computed. The shuffling method was used here as well.

Results

Part I: measuring noise and EIB in human EEG of SCZ and healthy controls

ERPs from EEG in auditory oddball task in of SCZ

To start, we first replicated ERP results in the auditory oddball task to verify the task and dataset. A two-way ANOVA was performed to analyze the effect of group (CON, SCZ) and stimulus (deviants, standards) on maximum amplitude between 300-600 ms. It (Fig. 2, top row) revealed that there was a statistically significant interaction between the effects of group and stimulus ($F(1,1) = 11.868$, $P = 8.551 \times 10^{-4}$). Simple main effects analysis showed that group did have a statistically significant effect on maximum amplitude ($F(1,1) = 26.769$, $P = 1.294 \times 10^{-6}$), as did stimulus ($F(1,1) = 60.519$, $P = 9.245 \times 10^{-12}$).

Therefore, the ERP results showed a significantly lower amplitude in the P300 in SCZ participants for deviant stimuli, with a difference between stimuli, and an interaction. This replicates findings from a previous study (Wolff et al. 2022).

SNR, signal, and noise in EEG of auditory oddball task in SCZ

Next, we aimed to replicate previous findings on lower SNR in SCZ (Winterer et al. 2000; Winterer and Weinberger 2004; Wolff et al. 2022). To do so, the SNR AUC between 0 and 200 ms at electrode Fp1 was calculated for both deviants and standards (Fig. 2, second row). A two-way ANOVA was performed to analyze the effect of group and stimulus. The ANOVA revealed that there was not a statistically significant interaction between the effects of group and stimulus ($F(1,1) = 0.253$, $P = 0.616$). Simple main effects analysis showed that group did have a statistically significant effect on SNR AUC ($F(1,1) = 12.389$, $P = 6.679 \times 10^{-4}$) whereas stimulus did not ($F(1,1) = 0.423$, $P = 0.517$).

After computing the comparisons between groups in their SNR, we wanted to determine if the significant differences found were due to a difference in signal, noise, or both. To do so, we again did a two-way ANOVA on the signal (Fig. 2, third row) and the noise (Fig. 2, bottom row) in the same electrode and time interval.

No effect of group ($F(1,1) = 2.081$, $P = 0.153$), stimulus ($F(1,1) = 0.169$, $P = 0.682$), or interaction between them ($F(1,1) = 0.247$, $P = 0.620$) was found in the signal AUC. In contrast, a significant effect of group ($F(1,1) = 4.343$, $P = 0.040$) was found in the noise AUC. There was no effect of stimulus ($F(1,1) = 0.059$, $P = 0.809$) nor interaction between them ($F(1,1) = 0.075$, $P = 0.785$). This finding shows that the difference in SNR between groups is due to a difference in noise, not in signal.

In sum, our SNR analysis replicated previous findings that participants with SCZ have a lower SNR than healthy controls. Furthermore, we showed that this lower SNR is due to higher noise, not lower signal, in the task.

fE/Ib in rest and two tasks of SCZ EEG

Next, to measure the EIB in EEG in resting state data and two task states, the *f*E/Ib (Bruining et al. 2020) was computed (Fig. 3). For statistical comparison of the *f*E/Ib in rest, oddball and gating, the electrode with the largest absolute difference between groups (CON minus SCZ) (column 3, white X) was chosen to analyze. Simple Wilcoxon rank sum tests (Fig. 3, fourth column violin plots) showed that there was no statistically significant difference at electrode FC6 between the *f*E/Ib in rest ($P = 0.136$), but there was a significant difference at electrode F3 in the oddball task ($P = 0.033$) and at electrode FC6 in the gating task ($P = 0.012$).

First, the relationship between rest and the auditory oddball task was measured. A two-way ANOVA was performed to analyze the effect of group (CON, SCZ) and condition (rest, task) on *f*E/I. The ANOVA revealed that there was not a statistically significant interaction between the effects of group and condition ($F(1,1) = 0.646$, $P = 0.424$). Simple main effects analysis showed that group did have a statistically significant effect on *f*E/I ($F(1,1) = 6.128$, $P = 0.015$), but that condition did not ($F(1,1) = 1.564$, $P = 0.214$).

Next, the relationship between rest and the auditory gating task was measured. A two-way ANOVA revealed no statistically significant interaction between the effects of group and condition ($F(1,1) = 0.096$, $P = 0.758$). Simple main effects analysis showed that group did have a statistically significant effect on *f*E/I ($F(1,1) = 9.920$, $P = 0.002$), as did condition ($F(1,1) = 5.110$, $P = 0.026$).

In sum, our findings in the *f*E/Ib show no difference between groups in rest, but a significant difference between groups in both oddball and gating tasks. The *f*E/Ib in both tasks was higher in the SCZ group indicating higher levels of excitation in SCZ (when compared with healthy subjects).

Part II: measuring the effect of noise on the EIB in a neural population network model

General background and simulations performed

Is the increased noise causally related to the increased excitation in the EIB of schizophrenia? To address this question, we here link those noise results with a neural population network simulation through the LFP. The LFP can be used as a proxy for the EEG signal (Glomb et al. 2022), and the average activity of the population of a neural network can be modeled by the LFP (Glomb et al. 2022). This suggests that the LFP can have a key role in cross-level noise processing by for instance transferring the impact of noise from the cellular population level to the cortical and systemic level.

We first examine neural population responses to varying strengths of noise current. A neural network consisting of 1024 pyramidal cells and 256 interneurons (4:1 ratio) was simulated. Noise receptor conductance was 3.1 nS for pyramidal cells

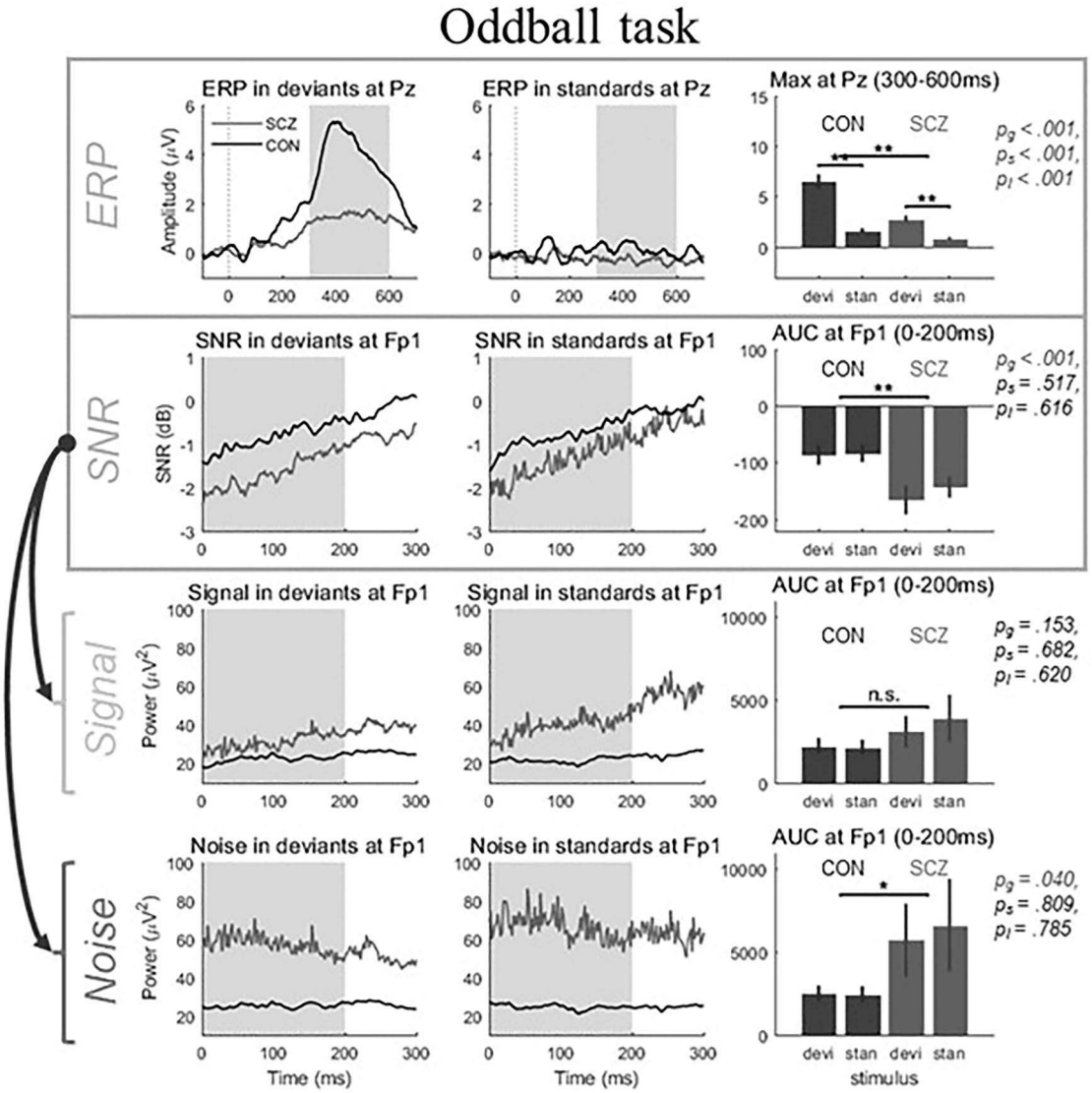

Fig. 2. ERPs and SNR in auditory oddball task. Top row: ERPs in deviants (left) and standards (middle), with bar plot (right), and ANOVA statistics on the maximum amplitude between 300 and 600 ms at electrode Pz (Jaworska et al. 2013). In the ERPs, it was found there was a significant effect of both group (p_g) and stimulus (p_s), and a significant interaction (p_i). Second row: SNR in deviants (left) and standards (middle), with bar plot (right), and ANOVA statistics on the area under the curve (AUC) between 0 and 200 ms at electrode Fp1 (Wolff et al. 2022). In the SNR AUC, a significant effect of group was found. There was no significant effect of stimulus, nor was there a significant interaction. As noted in the methods, the SNR is the ratio of two timeseries, the signal (third row) and the noise (bottom row). To determine, then, which of these components was significantly different between groups, they were independently examined. The signal at electrode Fp1 was investigated, and there was found to be no significant difference between groups or stimuli (third row, right bar plot). In contrast, there was found to be a significant difference between the healthy controls (CON) and schizophrenia participants (SCZ) in the noise (bottom row, right bar plot). Therefore, the difference in the SNR is due to a difference in noise, not signal. The line in each plot represents the mean for that specified group. Gray area: time interval during which the maximum amplitude (ERP) or AUC (SNR, signal, noise) were calculated. Box plots: CON = left bars, black; SCZ = right bars, gray. Error bars are standard error. *$P < 0.05$; **$P < 0.01$; n.s.: Not significant.

and 2.38 nS for interneurons. This was considered the baseline state (default network model) (Wang 1999; Compte et al. 2000; Calvin and Redish 2021). Simulations were done for five runs (each with distinct background noise) and results were averaged. Both populations show an asynchronous firing state in which individual neurons fire incoherently, leading to no particularly salient pattern in the network firing activity. The mean (±SD) SR is 4.68 ± 0.08 spikes/s for interneurons and 1.66 ± 0.09 spikes/s for pyramidal cells. This imitates the observed activity in such networks (Mazzoni et al. 2008).

In one set of simulations, we investigated how the changes in the noise current (the global change in the noise conductance, i.e. changing the conductance on both populations) affected the network activity, that is, the capacity of the network to respond to changes in the noise input current. The noise current was varied by altering receptor conductance in steps of 0.5 nS (1.6–8.1 nS for pyramidal cells, 0.38–7.38 nS for interneurons). Then, the NMDA current, EI ratio, SR, and LFP (as indices for different levels) were measured in response to varying strengths of noise current. Some of these changes, however, may restore the EIB, but changing the conductance of each population separately will change it. Therefore, in another set of simulations, we kept constant noise conductance for interneurons at 2.38 nS and varied pyramidal noise conductance. Here, we explore the NMDA current, EI ratio, SR, and LFP changes measured in pyramidal population in two sets of aforementioned simulations: (i) global changes of noise

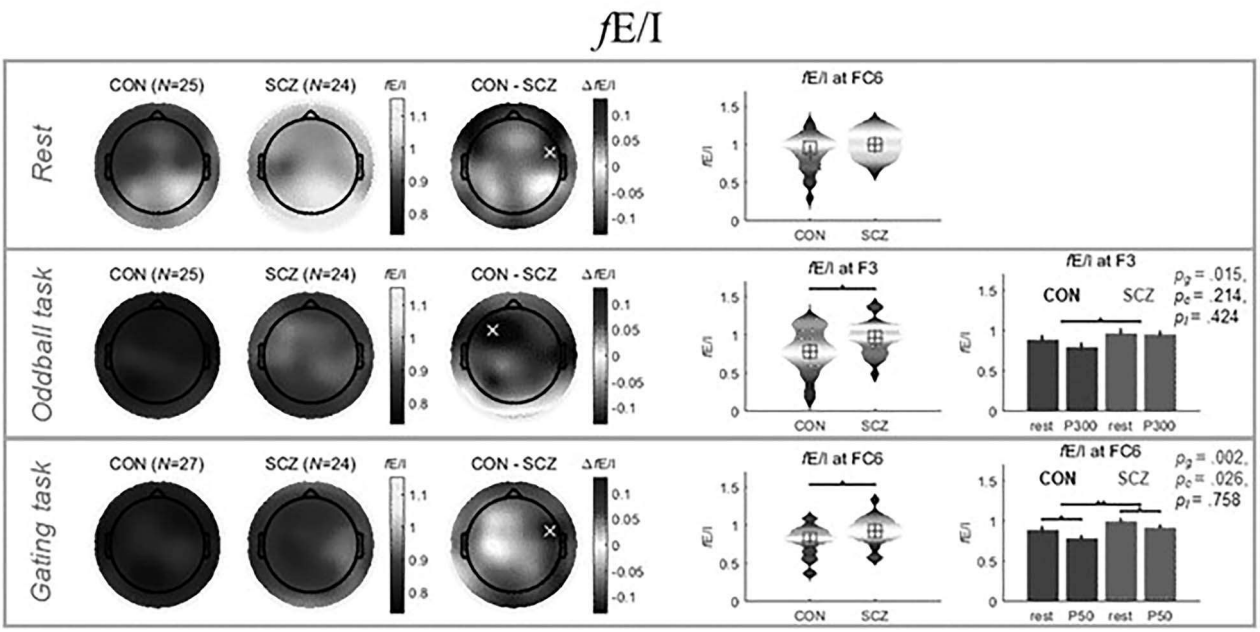

Fig. 3. ƒE/Ib as measured according to the methods of Bruining (Bruining et al. 2020). Three minutes of continuous EEG activity was measured in the resting state (Rest, top row), an auditory oddball task (Oddball task, second row), and an auditory gating task (Gating task, bottom row). The ƒE/I was measured in all 32 electrodes and plotted topographically (left three columns). From left to right, column 1 are healthy controls (CON), column 2 are schizophrenic participants (SCZ), and column 3 is the difference between them (CON—SCZ). Statistically, the electrode with the largest difference between groups (column 3, white X) was chosen to analyze. In Rest, at electrode FC6 there was no significant difference between groups. When comparing the EIB in rest and in task, an ANOVA (group, condition) was done (right column bar plots). For the Oddball task, a significant effect of group (p_g) was found. There was no significant effect of condition (p_c), nor was there a significant interaction (p_I). In the Gating task, there was a significant effect of group and condition, but no significant interaction. Violin plots: cross in the middle = mean; box = median. Box plots: CON = left bars, black; SCZ = right bars, gray. Error bars are standard error. $^*P < 0.05$; $^{**}P < 0.01$.

currents and (ii) just changing the noise applied to the pyramidal population.

Different levels of noise modulate the EIB and pyramidal population activity

As we expected, an increase in pyramidal noise conductance leads to an increase in the EI ratio, while an increase in the interneuron noise conductance shows a reduction in the EI ratio (Fig. 4A). However, for some changes in both parameters (pyramidal, interneuron noise conductance's), the EI ratio does not change compared with the baseline condition (as shown in black color in Fig. 4A). In Fig. 4(A), the area under the black curve shows increased EI ratio that corresponds to the EEG data presented above (whereas the area above the black curve depicts decreased EI ratio). We observed similar results for the NMDA current (Fig. 4B), LFP (Fig. 4C), and SR (supplement Fig. 2A).

In simulations with constant interneuron noise conductance, we observe that, with an increase in the pyramidal noise, the EI ratio in the pyramidal population increases monotonically (Fig. 4D). As noise is an excitatory input, it increases the NMDA currents (Fig. 4E), and as a result, the ratio of excitatory to inhibitory currents increases. Enhancing the input noise current to the pyramidal population elevates the NMDA current initially whereas for high levels of noise, the NMDA current saturates remaining roughly constant (Fig. 4E). For low levels of noise (corresponds to the conductance values < 2.6 nS in Fig. 4E), pyramidal cells do not fire action potentials; their NMDA current is therefore zero. With the increase in pyramidal noise conductance, the SR of the pyramidal population increases monotonically (Supplementary Fig. 2B). This finding aligns with previous research conducted by (Chance et al. 2002; Smirnova et al. 2015). For small values of pyramidal noise conductance (lower than 2.6 nS), the pyramidal population has no activity, and the SR is zero (Supplementary Fig. 2B). This may be due to a very low level of excitation input currents to the pyramidal cells, such that inhibitory inputs predominate (Fig. 4D). In this condition, NMDA current is zero as well (Fig. 4E).

Finally, the LFP was calculated as the sum of the absolute values of NMDA and GABA currents on the pyramidal population. In response to changes in pyramidal noise currents, the LFP increases initially, whereas for high levels of noise, the NMDA current shows very small changes (Fig. 4F) and exhibits a trend similar to the NMDA current (Fig. 4E).

In general, these results indicate higher responsivity of pyramidal population NMDA current, SR, EIB and LFP to higher strengths of noise current. This suggests a causal relationship between increased levels of excitation in EIB with increased degrees of noise.

We expect a decrease in SNR as the strength of noise increases. Thus, to evaluate the SNR, we administered the pulse depicted in Fig. 5(A) as the signal to the pyramidal population and quantified the SNR (Fig. 5C). Additionally, Fig. 5(B) represents the raster plot depicting the response of the pyramidal population to both the signal and background noise.

In addition to these simulations, we also examined the effect of reduction in GABA current which has been reported in SCZ (Vierling-Claassen et al. 2008; Anticevic et al. 2015). We repeated simulations with varying strengths of GABA current applied to each population. To reduce the GABA current, we decreased the GABA conductance in steps of 20% of the baseline condition (results are depicted in supplement Fig. 3). These results illustrate

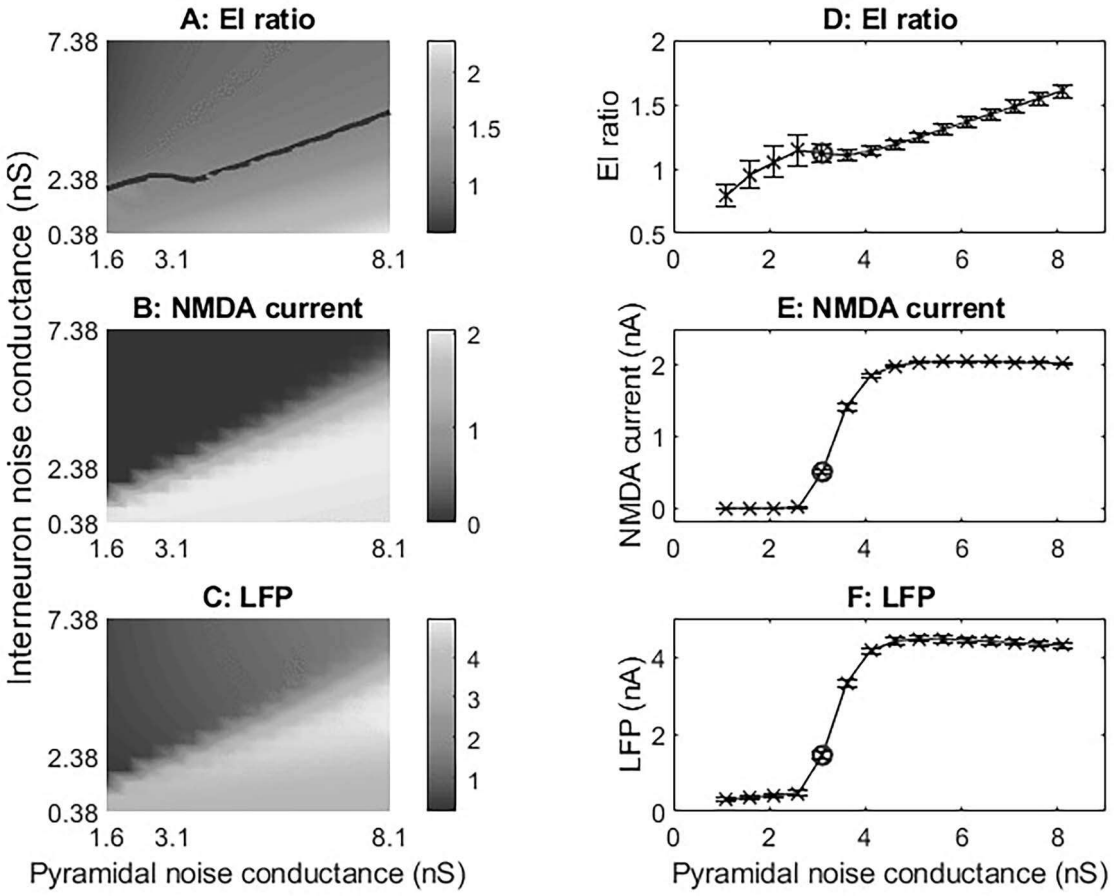

Fig. 4. Pyramidal population response to different levels of input noise current. (A), (B), and (C) show color maps as a function of pyramidal and interneuron noise conductance. (A) EI ratio; with an increase in pyramidal noise conductance, the EI ratio increases, and with an increase in interneuron noise conductance, the EI ratio decreases. With an increase in the noise conductance of both populations at some points, the EIB restores, which is depicted in black color. (B) NMDA current, and (C) LFP have similar changes to EI ratio. (D), (E), and (F) depict the same measurements as in (A), (B), and (C), respectively, as a function of just pyramidal noise conductance, and with constant interneuron noise conductance. (D) EI ratio; elevation in input noise increases the EI ratio. (E) NMDA current increases with an increase in input noise. (F) LFP increases in general; however, for high levels of noise, it changes in a small range. The circle shows baseline state, and error bars indicate ±SD. In some cases, SD is very small.

that by reducing the GABA current applied to the pyramidal population, the EI ratio, NMDA current, LFP, and SR increase because the pyramidal population receives less inhibitory currents and is thus more active. Additionally, the results indicate that under these conditions, the SNR decreases (Supplementary Fig. 4). However, decreasing GABA conductance of interneurons leads to their increased activity. Therefore, interneurons exert stronger inhibition on pyramidal cells, and this stronger inhibition then leads to decreased activity of these pyramidal cells with decreases (rather than increases) in the EIB and its excitatory component.

Cross-level relationships I—mediation analysis

In the next step, we need to assess how noise is related and transferred between the different levels, as indexed by our four measures. We hypothesized that noise changes the EIB, which, in turn, changes the other measures at both cellular population (NMDA) and cortical (LFP) levels. To investigate cross-level relationships, we, in the first step, used correlation and mediation analysis. To see correlations between these measures which represent different levels, Pearson's correlation coefficients between each pair and their *P*-values were computed (Table 2), and results showing all levels are correlated. In Table 2, those exhibiting significant correlations are highlighted.

These levels are not independent, but what is their relationship? To probe this, we focused on mediation analysis to investigate cross-level relationship of NMDA and LFP in mediating the effect of noise on EIB. We are interested in NMDA current, because it is a neural population level measurement and furthermore, based on NMDA hypothesis, it is associated with SCZ (Fišar 2022). Results reveal that (i) EI ratio has a total effect on NMDA current; (ii) there is a mediation (Fig. 6A and B); and (iii) the LFP is a mediator between them. Together, these results show that the LFP can mediate the effects of the EI ratio on NMDA current. One can thus say that the LFP can transfer the effect of noise from cortical levels to cellular population levels. Therefore, the LFP is mediator between different levels; this is further supported by their high correlation and MI.

Finally, a similar analysis was done for simulation results with reducing GABA current (shown in Supplementary Fig. 5). These results also confirm that the LFP can be mediators to transfer the effect of the EI ratio on NMDA current.

Cross-level relationships II—MI and DTW

The mediation analysis indicated the relationships between the NMDA current and LFP, and the key role of LFP and NMDA current in mediating between different levels to transfer the impact of noise. Results show that the LFP and NMDA current are correlated

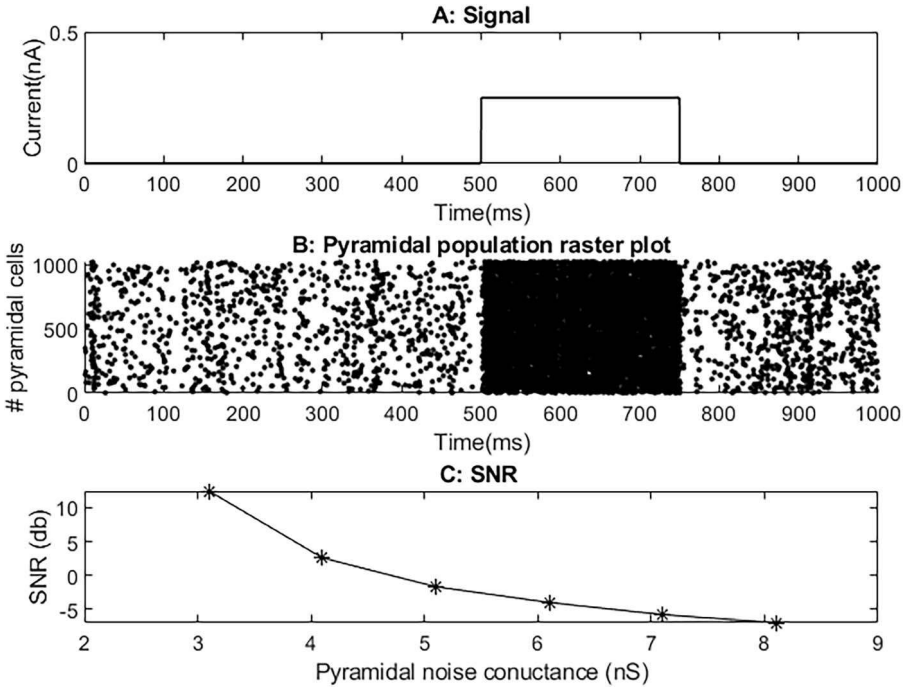

Fig. 5. SNR analysis. (A) Representation of the pulse used as the signal. (B) Raster plot illustrating the response of the pyramidal population to the background noise and the signal depicted in (A). (C) Relationship between the SNR and the strength of the background noise, demonstrating a decrease in SNR as the background noise increases.

Table 2. Pearson's correlation coefficients between each pair of NMDA current, EI ratio, SR, and LFP in response to different strength of noise current applied to the pyramidal population; $^{*}P < 0.05$, $^{**}P < 0.01$, $^{***}P < 0.001$.

	NMDA	EI ratio	SR	LFP
NMDA	1	**0.776*****	**0.799** ***	**0.999*****
EI ratio		1	**0.937** ***	**0.763*****
SR			1	**0.777*****
LFP				1

and that the LFP can transfer the effects of higher levels on the NMDA current. Here, to substantiate the relationship between the NMDA current and LFP, we computed the MI between them for each set of simulations.

So, global change in noise current (i.e. changing noise conductance of both populations) gave a matrix (for simulations shown in the left column in Fig. 4) or a sequence (for the right column in Fig. 4, one for NMDA current and one for LFP). Then, the MI between them was computed to confirm their interdependence. Here, the order of the sequences represents different strengths of noise.

To further strengthen the MI results, we also shuffled the NMDA and LFP, and calculated MI between the original NMDA current and shuffled version of LFP and vice versa and both shuffled. To shuffle the LFP or NMDA, we changed the order of the LFP or NMDA sequence randomly. We shuffled 1000 times, each time the MI between the original NMDA/LFP and shuffled LFP/NMDA was measured. At the end, we had a sequence of 1,000 MI values. The boxplot was plotted. Results are presented in Fig. 6(C) and (E). As seen in Fig. 7(C) and (E), the LFP and NMDA have a high MI (original in Fig), while shuffling reduces their MI (*P*-value*P*-value < 0.05). This indicates that NMDA current and LFP are related to each other in a systematic way with respect to specific levels of noise.

To confirm the MI results, DTW which is a distance-based measurement of similarity (Tao et al. 2021) was also computed for this simulation. DTW results are shown in Fig. 6(D) and (F). Lower values of DTW correspond to higher similarity. DTW results confirm the MI; the NMDA current and LFP have high similarity, which decreases with shuffling. The MI and DTW were also computed for simulation results with GABA conductance reduction (results are illustrated in Supplementary Fig. 6). This supports our finding that shuffling reduces the MI in a significant way (*P*-value<0.05).

Discussion

SCZ patients show sensory impairments, and previous EEG studies suggest that these are closely related to lower SNR due to higher noise in the neural activity of SCZ. In this context, noise is considered the ongoing spontaneous neural activity unrelated to the stimulus while signal is considered the neural activity evoked by the stimulus during the task. Despite the findings in these EEG studies, the mechanism underlying increased noise in SCZ is unknown. To connect increased noise with known abnormalities in EIB in SCZ, we ask if the increased noise in SCZ is related to increasing degrees of excitation in EIB. To answer this, we here combined human empirical EEG with computational modeling to investigate the mechanisms of increased noise in SCZ.

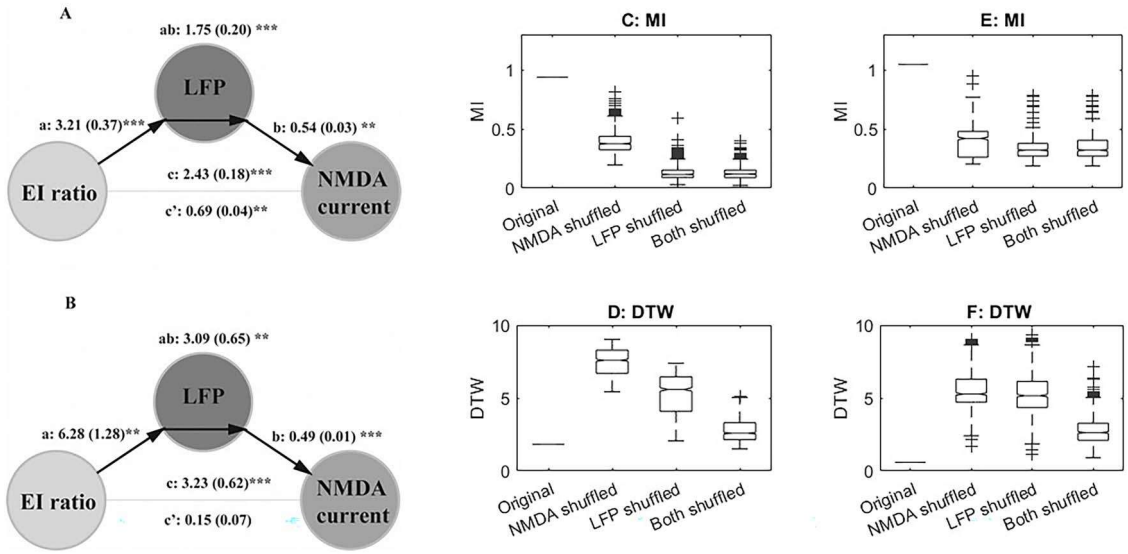

Fig. 6. Mediation and cross level analyses. (A) and (B) depict the results of mediation analysis; with coefficients of paths (*a*: coefficient from *x* to *m*; *b*: from *m* to *y*; *c*': direct coefficient from *x* to *y*; *ab*: indirect coefficient from *x* to *y*; *c*: total effect) shown along with standard errors in parentheses. (A) shows mediation analysis with changing the noise conductance on both populations, where the LFP mediates between excitation and inhibition ratio and NMDA current. (B) shows the same analysis as in (A), with variable pyramidal noise conductance and constant interneuron noise conductance. $^{*}P < 0.05$, $^{**}P < 0.01$, $^{***}P < 0.001$. (C)–(F) display MI and DTW between NMDA current and LFP. (C) and (D) show MI and DTW as a function of both populations noise conductance. (C) shows MI between NMDA current (original) and their shuffled versions, where the original MI differs significantly from MI between the shuffled versions of NMDA current or LFP or both (*P*-value < 0.05). Shuffling reduces MI. (D) shows DTW between NMDA current and LFP, where shuffling significantly reduces their similarity (*P*-value < 0.05). The medians are shown, and data points beyond the whiskers are displayed using +. Shuffling was done by randomly changing the order of the sequence of LFP or NMDA to decorrelate their alignment. (E) and (F) show the same analysis as in (C) and (D), respectively, but as a function of pyramidal noise conductance and with constant interneuron noise conductance.

We first show significantly reduced SNR and increased noise in SCZ in our EEG auditory oddball task data, thus confirming previous findings (Winterer et al. 2000; Wolff et al. 2022). As we showed significantly lower SNR across both stimuli in the SCZ participants, we next had to determine if this was due to increased noise or decreased signal. This second analysis separated the SNR into its respective components and found no difference between groups in signal but a significant increase in noise across both stimuli in the SCZ group. This showed that the decreased SNR was in fact due to increased noise, and that it was not specific to task-relevant or -irrelevant stimuli.

Next, we demonstrate, for the first time, abnormal EIB on the systemic level of EEG by measuring the *f*E/Ib (Bruining et al. 2020) in SCZ participants and healthy controls during rest and two tasks. We found no significant difference in *f*E/Ib in the resting state, but a significant difference between groups in both the auditory oddball and gating tasks was found, with a higher level of excitation in the *f*E/Ib in SCZ. These findings show a rest-task difference between groups which has been shown previously (Northoff and Gomez-Pilar 2021) and suggests a relationship of increased noise and abnormal EIB in SCZ.

But is there a causal relationship between noise and EIB? Though this cannot be shown in the EEG data, our computational simulations allowed us to test this. The neural population network simulation shows that higher strengths of input noise on the network pyramidal population leads to higher levels of excitation in the EIB ratio, a stronger LFP, a higher SR, and higher NMDA current (Fig. 4 and Supplementary Fig. 2). This suggests a causal relationship between noise and both the EIB and LFP within the simulation. Importantly, these findings converge with and extends the observed EIB changes in EEG. Hence, we infer that the parallel changes in noise and EIB observed in EEG are causally related, with increasing degrees of noise leading to increasingly abnormal EIB tilted toward the excitatory pole.

In addition, in its relationship to input noise, the slope of the increase in the NMDA current is initially high and then become roughly constant (as NMDA receptors saturate) (Lester and Jahr 1992; Ishikawa et al. 2002; Cummings and Popescu 2015). Given that NMDA is known to mediate excitation (Furukawa et al. 2005), we suppose that the increased excitation in the EIB is related to the increase in the NMDA current. Interestingly, analogous to the input-NMDA curve, we observed a more or less similar relationship of the LFP with the input noise; this is even more sensible given that the LFP are known to be shaped by synaptic inputs (Sinha and Narayanan 2022) as from NMDA. Together, these findings suggest cross-level interaction of NMDA and LFP in the shaping of the excitatory component of the EIB by increasing degrees of noise (Marsman et al. 2013; Schobel et al. 2013).

In order to further investigate cross-level relationships, we combined different analyses including correlation, mediation model, and MI/ DTW. We observed a key role of the LFP on mediating the impact of noise on the cellular population level of NMDA. Given that the LFP operate on a cortical level and NMDA on the cellular population level, one can speak of a cross-level bottom-up modulation.

This cross-level relationship carries major implications. Increased noise may be prevalent at the cortical level of the LFP in SCZ as documented and supported by our EEG findings. That, in turn, may affect the cellular population level NMDA activity as seen in increased NMDA current. Future studies are needed to investigate whether SCZ is characterized by a primary deficit in NMDA, which, through top-down modulation, changes the EIB and subsequently the LFP. Or, alternatively, SCZ may be featured by a primary change in its dynamics as, for instance, increased temporal imprecision (Adams et al. 2013;

Karanikolaou et al. 2022; Wolff et al. 2022) of the LFP, which, through bottom-up modulation, changes NMDA.

At the same time, there might be top-down modulation. Support for such top-down modulation comes from a recent animal study (Saunders et al. 2012). It found that exposure to NMDA receptor antagonists' ketamine and MK-801 lead to a dose-dependent increase in high (35–80 Hz) frequency baseline power, but a decrease in high frequency evoked and total power. This resulted in lower SNR in this frequency range which was due to higher noise, namely baseline spontaneous activity (i.e. non-related task activity). The findings of this study are consistent with our EEG results and previous work (Winterer et al. 2000; Winterer and Weinberger 2004; Wolff et al. 2022) as they found higher baseline power (noise) and lower signal (evoked activity) with increased blocking of NMDA receptors. Along with the known dopaminergic dysfunction in SCZ (Winterer and Weinberger 2004; Rolls et al. 2008; Howes et al. 2015; Grace and Gomes 2019), NMDA relates to dopamine as their projections overlap and converge in the brain (Wang et al. 2012). Accordingly, our findings lend further evidence to the glutamate and NMDA hypotheses of SCZ (Moghaddam and Javitt 2012), as well as, albeit indirectly, to the dopamine model of psychosis (Tost et al. 2010; Kesby et al. 2018; Novak and Seeman 2022).

Our study had some limitations. In the EEG data, one limitation was the use of one dataset and task for the SNR analysis, and the relatively modest sample sizes for each group. Furthermore, greater granularity would have been possible in the *f*E/Ib topoplots if there had been more than 32 electrodes in our dataset. This must be explored in future studies. We also simulated the homogeneous network with no spatial dimension, and heterogeneity in the network was not considered. Future studies could include heterogeneity in the network. In addition, our study probed the cross-level relationship in response to the noise using modeling approaches and illustrated the key role of the LFP as the bridge between different levels. However, empirical data at the cellular level, e.g. NMDA current and the LFP may want to be included in the future in our computational model.

Conclusion

In conclusion, we demonstrate a close relationship between increased noise and increasing degrees of excitation in the EIB of SCZ. Conjoining EEG data and computational modeling allows us to draw a cross-level relationship from the cellular population level of NMDA over the EIB to the LFP as measured in EEG. We show that increased noise in neural activity reverberates through all levels, with the LFP exerting bottom-up modulation of the NMDA current. This provides insight into the cross-level neuronal and computational mechanisms of increased noise and its modulation of the EIB in SCZ. That aligns well with and extends current biochemical models of SCZ, of which the NMDA-hypothesis is the most prominent.

Author contributions

Samira Abbasi (Conceptualization, Formal analysis, Methodology, Resources, Software, Validation, Visualization, Writing—original draft, Writing—review and editing), Annemarie Wolff (Conceptualization, Formal analysis, Methodology, Resources, Software, Validation, Visualization, Writing—review and editing), Yasir Çatal (Writing—review and editing), Georg Northoff (Conceptualization, Funding acquisition, Investigation, Project administration, Resources, Supervision, Validation, Writing—review and editing).

Supplementary material

Supplementary material is available at *Cerebral Cortex* online.

Funding

This research has received funding from the European Union's Horizon 2020 Framework Program for Research and Innovation under the Specific Grant Agreement No. 785907 (Human Brain Project SGA2). G.N. is grateful for funding provided by UMRF, uOBMRI, CIHR, and PSI.

Conflict of interest statement: The authors declare that they have no conflict of interest.

Data availability

Modelling and analysis scripts are available upon request, via email, to the authors. The data that support the findings of this study are available from the authors, but restrictions apply to the availability of these data, which were used under the approval of the Research Ethics Board of the Institute of Mental Health Research (Ottawa) for the current study, and so are not publicly available. Data are, however, available from the authors upon reasonable request and with permission from the Research Ethics Board of the Institute of Mental Health Research (Ottawa).

References

Adams RA, Stephan KE, Brown HR, Frith CD, Friston KJ. The computational anatomy of psychosis. *Frontiers Psychiatry*. 2013:4:47.

Adams RA, Pinotsis D, Tsirlis K, Unruh L, Mahajan A, Horas AM, Convertino L, Summerfelt A, Sampath H, Du XM. Computational modeling of electroencephalography and functional magnetic resonance imaging paradigms indicates a consistent loss of pyramidal cell synaptic gain in schizophrenia. *Biol Psychiatry*. 2022:91(2):202–215.

Anticevic A, Murray JD, Barch DM. Bridging levels of understanding in schizophrenia through computational modeling. *Clin Psychol Sci*. 2015:3(3):433–459.

Bigdely-Shamlo N, Mullen T, Kothe C, Su K-M, Robbins KA. The prep pipeline: standardized preprocessing for large-scale EEG analysis. *Fron Neuroinform*. 2015:9:16.

Braun W, Matsuzaka Y, Mushiake H, Northoff G, Longtin A. Non-additive activity modulation during a decision making task involving tactic selection. *Cogn Neurodyn*. 2022:16(1):117–133.

Bruining H, Hardstone R, Juarez-Martinez EL, Sprengers J, Avramiea A-E, Simpraga S, Houtman SJ, Poil S-S, Dallares E, Palva S. Measurement of excitation-inhibition ratio in autism spectrum disorder using critical brain dynamics. *Sci Rep*. 2020:10(1):1–15.

Brunel N. Dynamics of sparsely connected networks of excitatory and inhibitory spiking neurons. *J Comput Neurosci*. 2000:8:183–208.

Buzsáki G, Anastassiou CA, Koch C. The origin of extracellular fields and currents—EEG, ECOG, LFP and spikes. *Nat Rev Neurosci*. 2012:13(6):407–420.

Calvin OL, Redish AD. Global disruption in excitation-inhibition balance can cause localized network dysfunction and schizophrenia-like context-integration deficits. *PLoS Comput Biol*. 2021:17(5):e1008985.

Chance FS, Abbott LF, Reyes AD. Gain modulation from background synaptic input. *Neuron*. 2002:35(4):773–782.

Choueiry J, Blais CM, Shah D, Smith D, Fisher D, Labelle A, Knott V. Combining CDP-choline and galantamine, an optimized $\alpha 7$

nicotinic strategy, to ameliorate sensory gating to speech stimuli in schizophrenia. *Int J Psychophysiol*. 2019:145:70–82.
Compte A, Brunel N, Goldman-Rakic PS, Wang X-J. Synaptic mechanisms and network dynamics underlying spatial working memory in a cortical network model. *Cereb Cortex*. 2000:10(9):910–923.
Cummings KA, Popescu GK. Glycine-dependent activation of NMDA receptors. *J Gen Physiol*. 2015:145(6):513–527.
Dalal T, Haddad R. Upstream γ-synchronization enhances odor processing in downstream neurons. *Cell Rep*. 2022:39(3):110693.
Davenport EC, Szulc BR, Drew J, Taylor J, Morgan T, Higgs NF, López-Doménech G, Kittler JT. Autism and schizophrenia-associated CYFIP1 regulates the balance of synaptic excitation and inhibition. *Cell Rep*. 2019:26(8):2037–2051.e2036.
David O, Kilner JM, Friston KJ. Mechanisms of evoked and induced responses in MEG/EEG. *NeuroImage*. 2006:31(4):1580–1591.
Deco G, Ponce-Alvarez A, Hagmann P, Romani GL, Mantini D, Corbetta M. How local excitation–inhibition ratio impacts the whole brain dynamics. *J Neurosci*. 2014:34(23):7886–7898.
Delorme A, Makeig S. Eeglab: an open source toolbox for analysis of single-trial EEG dynamics including independent component analysis. *J Neurosci Methods*. 2004:134(1):9–21.
Dimitrov AG, Lazar AA, Victor JD. Information theory in neuroscience. *J Comput Neurosci*. 2011:30(1):1–5.
Faisal AA, Selen LP, Wolpert DM. Noise in the nervous system. *Nat Rev Neurosci*. 2008:9(4):292–303.
Fišar Z. Biological hypotheses, risk factors, and biomarkers of schizophrenia. *Prog Neuro-Psychopharmacol Biol Psychiatry*. 2022:120:110626.
Friston K. Computational psychiatry: from synapses to sentience. *Mol Psychiatry*. 2022:1-13(1):256–268.
Friston KJ, Bastos AM, Pinotsis D, Litvak V. LFP and oscillations—what do they tell us? *Curr Opin Neurobiol*. 2015:31:1–6.
Furukawa H, Singh SK, Mancusso R, Gouaux E. Subunit arrangement and function in NMDA receptors. *Nature*. 2005:438(7065):185–192.
Gerstner W, Kistler WM. *Spiking neuron models: single neurons, populations, plasticity*. Cambridge University Press, UK; 2002.
Glomb K, Cabral J, Cattani A, Mazzoni A, Raj A, Franceschiello B. Computational models in electroencephalography. *Brain Topogr*. 2022:35(1):142–161.
Grace AA, Gomes FV. The circuitry of dopamine system regulation and its disruption in schizophrenia: insights into treatment and prevention. *Schizophr Bull*. 2019:45(1):148–157.
Howes O, McCutcheon R, Stone J. Glutamate and dopamine in schizophrenia: an update for the 21st century. *J Psychopharmacol*. 2015:29(2):97–115.
Ishikawa T, Sahara Y, Takahashi T. A single packet of transmitter does not saturate postsynaptic glutamate receptors. *Neuron*. 2002:34(4):613–621.
Jami SA, Cameron S, Wong JM, Daly ER, McAllister AK, Gray JA. Increased excitation-inhibition balance and loss of gabaergic synapses in the serine racemase knockout model of NMDA receptor hypofunction. *J Neurophysiol*. 2021:126(1):11–27.
Javitt DC. Sensory processing in schizophrenia: neither simple nor intact. *Schizophr Bull*. 2009:35(6):1059–1064.
Javitt DC, Freedman R. Sensory processing dysfunction in the personal experience and neuronal machinery of schizophrenia. *Am J Psychiatry*. 2015:172(1):17–31.
Jaworska N, De Somma E, Blondeau C, Tessier P, Norris S, Fusee W, Smith D, Blier P, Knott V. Auditory p3 in antidepressant pharmacotherapy treatment responders, non-responders and controls. *Eur Neuropsychopharmacol*. 2013:23(11):1561–1569.
Jaworska N, Wang H, Smith DM, Blier P, Knott V, Protzner AB. Pre-treatment EEG signal variability is associated with treatment success in depression. *NeuroImage: Clinical*. 2018:17:368–377.
Karanikolaou M, Limanowski J, Northoff G. Does temporal irregularity drive prediction failure in schizophrenia? Temporal modelling of ERPS. *Schizophrenia*. 2022:8(1):1–9.
Kehrer C, Maziashvili N, Dugladze T, Gloveli T. Altered excitatory-inhibitory balance in the NMDA-hypofunction model of schizophrenia. *Front Mol Neurosci*. 2008:6:226–233.
Kenny DA, Korchmaros JD, Bolger N. Lower level mediation in multilevel models. *Psychol Methods*. 2003:8(2):115–128.
Kesby J, Eyles D, McGrath J, Scott J. Dopamine, psychosis and schizophrenia: the widening gap between basic and clinical neuroscience. *Transl Psychiatry*. 2018:8(1):1–12.
Kraskov A, Stögbauer H, Grassberger P. Estimating mutual information. *Phys Rev E*. 2004:69(6):066138.
Lakatos P, O'Connell MN, Barczak A, Mills A, Javitt DC, Schroeder CE. The leading sense: Supramodal control of neurophysiological context by attention. *Neuron*. 2009:64(3):419–430.
Lakatos P, Schroeder CE, Leitman DI, Javitt DC. Predictive suppression of cortical excitability and its deficit in schizophrenia. *J Neurosci*. 2013:33(28):11692–11702.
Lam NH, Borduqui T, Hallak J, Roque A, Anticevic A, Krystal JH, Wang X-J, Murray JD. Effects of altered excitation-inhibition balance on decision making in a cortical circuit model. *J Neurosci*. 2022:42(6):1035–1053.
Ledoux E, Brunel N. Dynamics of networks of excitatory and inhibitory neurons in response to time-dependent inputs. *Front Comput Neurosci*. 2011:5:25.
Lemardelet L, Caron P-O. Illustrations of serial mediation using PROCESS, Mplus and R. *Quant Methods Psychol*. 2022:18(1):66–90.
Lester RA, Jahr CE. NMDA channel behavior depends on agonist affinity. *J Neurosci*. 1992:12(2):635–643.
Marsman A, Van Den Heuvel MP, Klomp DW, Kahn RS, Luijten PR, Hulshoff Pol HE. Glutamate in schizophrenia: a focused review and meta-analysis of ^{1}H-MRS studies. *Schizophr Bull*. 2013:39(1):120–129.
Martínez A, Gaspar PA, Hillyard SA, Bickel S, Lakatos P, Dias EC, Javitt DC. Neural oscillatory deficits in schizophrenia predict behavioral and neurocognitive impairments. *Front Hum Neurosci*. 2015:9:371.
Martínez-Cañada P, Ness TV, Einevoll GT, Fellin T, Panzeri S. Computation of the electroencephalogram (EEG) from network models of point neurons. *PLoS Comput Biol*. 2021:17(4):e1008893.
Mazzoni A, Panzeri S, Logothetis NK, Brunel N. Encoding of naturalistic stimuli by local field potential spectra in networks of excitatory and inhibitory neurons. *PLoS Comput Biol*. 2008:4(12):e1000239.
Mazzoni A, Whittingstall K, Brunel N, Logothetis NK, Panzeri S. Understanding the relationships between spike rate and delta/gamma frequency bands of LPFs and EEGs using a local cortical network model. *NeuroImage*. 2010:52(3):956–972.
Mazzoni A, Brunel N, Cavallari S, Logothetis NK, Panzeri S. Cortical dynamics during naturalistic sensory stimulations: experiments and models. *J Physiol-Paris*. 2011:105(1–3):2–15.
Moghaddam B, Javitt D. From revolution to evolution: the glutamate hypothesis of schizophrenia and its implication for treatment. *Neuropsychopharmacology*. 2012:37(1):4–15.
Molina V, Bachiller A, Suazo V, Lubeiro A, Poza J, Hornero R. Noise power associated with decreased task-induced variability of brain electrical activity in schizophrenia. *Eur Arch Psychiatry Clin Neurosci*. 2016:266(1):55–61.
Mullen T. Nitrc: Cleanline: tool/resource info. Repéré à https://wwwnitrc.org/projects/cleanline. 2012.

Murray JD, Anticevic A, Gancsos M, Ichinose M, Corlett PR, Krystal JH, Wang X-J. Linking microcircuit dysfunction to cognitive impairment: effects of disinhibition associated with schizophrenia in a cortical working memory model. *Cereb Cortex*. 2014:24(4): 859–872.

Narendran R, Mason NS, Himes ML, Frankle WG. Imaging cortical dopamine transmission in cocaine dependence: a [^{11}C] FLB 457–amphetamine positron emission tomography study. *Biol Psychiatry*. 2020:88(10):788–796.

Northoff G, Gomez-Pilar J. Overcoming rest–task divide—abnormal temporospatial dynamics and its cognition in schizophrenia. *Schizophr Bull*. 2021:47(3):751–765.

Novak G, Seeman MV. Dopamine, psychosis, and symptom fluctuation: a narrative review. *Healthcare*. 2022: MDPI:10(9):1713.

Nunez PL, Srinivasan R. *Electric fields of the brain: the neurophysics of EEG*. Oxford University Press, USA; 2006.

Palaniyappan L, Simmonite M, White TP, Liddle EB, Liddle PF. Neural primacy of the salience processing system in schizophrenia. *Neuron*. 2013:79(4):814–828.

Qian N, Lipkin RM, Kaszowska A, Silipo G, Dias EC, Butler PD, Javitt DC. Computational modeling of excitatory/inhibitory balance impairments in schizophrenia. *Schizophrenia Res*. 2020:249: 47–55.

Rolls ET, Loh M, Deco G, Winterer G. Computational models of schizophrenia and dopamine modulation in the prefrontal cortex. *Nat Rev Neurosci*. 2008:9(9):696–709.

Salvador S, Chan P. Toward accurate dynamic time warping in linear time and space. *Intell Data Anal*. 2007:11(5):561–580.

Saunders JA, Gandal MJ, Siegel SJ. NMDA antagonists recreate signal-to-noise ratio and timing perturbations present in schizophrenia. *Neurobiol Dis*. 2012:46(1):93–100.

Schobel SA, Chaudhury NH, Khan UA, Paniagua B, Styner MA, Asllani I, Inbar BP, Corcoran CM, Lieberman JA, Moore H. Imaging patients with psychosis and a mouse model establishes a spreading pattern of hippocampal dysfunction and implicates glutamate as a driver. *Neuron*. 2013:78(1):81–93.

Shrout PE, Bolger N. Mediation in experimental and nonexperimental studies: new procedures and recommendations. *Psychol Methods*. 2002:7(4):422–445.

Sinha M, Narayanan R. Active dendrites and local field potentials: biophysical mechanisms and computational explorations. *Neurosci*. 2022:489:111–142.

Smirnova EY, Zaitsev AV, Kim KK, Chizhov AV. The domain of neuronal firing on a plane of input current and conductance. *J Comput Neurosci*. 2015:39:217–233.

Sohal VS, Rubenstein JL. Excitation-inhibition balance as a framework for investigating mechanisms in neuropsychiatric disorders. *Mol Psychiatry*. 2019:24(9):1248–1257.

Tao Y, Both A, Silveira RI, Buchin K, Sijben S, Purves RS, Laube P, Peng D, Toohey K, Duckham M. A comparative analysis of trajectory similarity measures. *GIScience Remote Sens*. 2021:58(5): 643–669.

Thoenes S, Oberfeld D. Meta-analysis of time perception and temporal processing in schizophrenia: differential effects on precision and accuracy. *Clin Psychol Rev*. 2017:54:44–64.

Timme NM, Lapish C. A tutorial for information theory in neuroscience. *Eneuro*. 2018:5(3):ENEURO.0052–ENEU18.2018.

Tost H, Alam T, Meyer-Lindenberg A. Dopamine and psychosis: theory, pathomechanisms and intermediate phenotypes. *Neurosci Biobehav Rev*. 2010:34(5):689–700.

Vierling-Claassen D, Siekmeier P, Stufflebeam S, Kopell N. Modeling GABA alterations in schizophrenia: a link between impaired inhibition and altered gamma and beta range auditory entrainment. *J Neurophysiol*. 2008:99(5):2656–2671.

Wang X-J. Synaptic basis of cortical persistent activity: the importance of NMDA receptors to working memory. *J Neurosci*. 1999:19(21):9587–9603.

Wang M, Wong AH, Liu F. Interactions between NMDA and dopamine receptors: a potential therapeutic target. *Brain Res*. 2012:1476: 154–163.

Webb GI, Petitjean F. Tight lower bounds for dynamic time warping. *Pattern Recogn*. 2021:115:107895.

White JA, Rubinstein JT, Kay AR. Channel noise in neurons. *Trends Neurosci*. 2000:23(3):131–137.

Winkler I, Haufe S, Tangermann M. Automatic classification of artifactual ICA-components for artifact removal in EEG signals. *Behav Brain Funct*. 2011:7(1):30.

Winkler I, Brandl S, Horn F, Waldburger E, Allefeld C, Tangermann M. Robust artifactual independent component classification for BCI practitioners. *J Neural Eng*. 2014:11(3):035013.

Winterer G, Weinberger DR. Genes, dopamine and cortical signal-to-noise ratio in schizophrenia. *Trends Neurosci*. 2004:27(11):683–690.

Winterer G, Ziller M, Dorn H, Frick K, Mulert C, Dahhan N, Herrmann W, Coppola R. Cortical activation, signal-to-noise ratio and stochastic resonance during information processing in man. *Clin Neurophysiol*. 1999:110(7):1193–1203.

Winterer G, Ziller M, Dorn H, Frick K, Mulert C, Wuebben Y, Herrmann W, Coppola R. Schizophrenia: reduced signal-to-noise ratio and impaired phase-locking during information processing. *Clin Neurophysiol*. 2000:111(5):837–849.

Winterer G, Coppola R, Goldberg TE, Egan MF, Jones DW, Sanchez CE, Weinberger DR. Prefrontal broadband noise, working memory, and genetic risk for schizophrenia. *Am J Psychiatry*. 2004:161(3): 490–500.

Wolff A, Gomez-Pilar J, Zhang J, Choueiry J, de la Salle S, Knott V, Northoff G. It's in the timing: reduced temporal precision in neural activity of schizophrenia. *Cereb Cortex*. 2022:32(16):3441–3456.

Zou X, Wang D-H. On the phase relationship between excitatory and inhibitory neurons in oscillation. *Front Comput Neurosci*. 2016:10:138.